Thermo-electrical characterization of PZT ferroelectric capacitors

Author: Pelayo Marín Villa[1] and Advisor: Salvador Dueñas Carazo[1]

Departamento de Electricidad y Electrónica, Universidad de Valladolid, E-47011 Valladolid, Spain.

(Dated: 23 July 2020)

Abstract

Este trabajo versa sobre la caracterización termo-eléctrica de dos diafragmas piezoeléctricos, conocidos coloquialmente como zumbadores, cuyos elementos activos son cerámicas de titanato de zirconato de plomo (PZT). En primer lugar, realizamos un estudio de las curvas intensidad-voltaje y los ciclos de histéresis de los zumbadores para, posteriormente, proceder al análisis de rendimiento de las muestras a lo largo de un rango ancho de temperaturas. Logramos demostrar que, a medida que la temperatura descendía, la cerámica requería de un voltaje mayor para polarizarse completamente y que las corrientes de polarización disminuían. Encontramos también que el campo coercitivo aumentaba notablemente hacia menores temperaturas, con lo que aumentaban las pérdidas del dieléctrico (dadas por el área bajo la curva del ciclo de histéresis). La explicación para este fenómeno reside en que el cambio de polarización en el material ferroeléctrico viene dado primordialmente por el movimiento de las paredes de dominio, un proceso activado térmicamente. El estudio del backswitching de la polarización demostró que existía una dependencia con el tamaño, si bien el comportamiento con la temperatura en ambas muestras era similar. Posteriormente, caracterizamos en frecuencia y temperatura la impedancia eléctrica de uno de los zumbadores, así como la capacidad y su permitividad eléctrica. Finalmente, puesto que los zumbadores se utilizan como componentes acústicos, procedimos a utilizar un sonómetro con ánimo de medir la presión sonora a temperatura ambiente. Este análisis confirmó sus excelentes propiedades electroacústicas en el rango de frecuencias perceptibles por el oído humano medio (20 Hz - 20 kHz).

Keywords: PZT, ferroelectricity, polarization backswitching, piezoelectricity, impedance analysis.

I. CONTEXT AND INTRODUCTION

Piezoelectricity is a phenomenon exhibited by certain materials which indicates a coupling between mechanical and electrical properties. Thus, the average electric polarization of a substance can be different than zero due to the application of mechanical stress. The brothers Pierre and Jacques Curie were the first researchers to publish their findings on certain crystals[1], but it wasn't until 1917 when the team led by Paul Langevin first took advantage of the piezoelectricity of quartz designing and developping the world's first sonar[2]. The success of this system led to a fast development of novel applications and the discovery of a good number of crystals that share this phenomenon.

During the Second World War, several independent groups from the United States of America, the Soviet Union and Japan created synthetic ceramics, such as the family of lead zirconate titanate $Pb[Zr_xTi_{1-x}]O_3$ (shortened as PZT), whose piezoelectrical properties were significantly better than those available so far, despite it was Joseph Vasalek who first identified a simmilar behavior in Rochelle salt in 1920[3]. The name *ferroelectrics* was

coined for this special class of piezoelectric materials due to the existance of two or more discrete metastable states of non-zero electric polarization when no electric field is externally applied, featuring a spontaneous polarization and the hysteresis phenomenon[4].

Piezoelectric diaphragms, commonly known as buzzers, are electroacoustic components which take advantage of their inverse piezoelectric effect[5]; when an electric field is applied in the polarization direction of the material, the latter produces a mechanical deformation in the opposite direction, resulting in a human-audible sound in the case of buzzers[6]. Their most common application so far has been the integration of alarm systems. Moreover, their range of application has increased over the years, and recent studies propose piezoelectric diaphragms as possible sensors for Structural Health Monitoring (SHM)[7−9]. Silva de Freitas et al.[10,11] studied PZT buzzers' application in SHM as damage detectors, studying both their temperature stability and their temperature-frequency dependence from 0 to 70 °C.

Several studies have already been performed on lead magnesium niobate-lead titanate (PMN-

PT) piezoelectric crystals[12] and lead-free ceramics such as $0.965(K_{0.45}Na_{0.55})(Nb_{0.96}Sb_{0.04})O_3$-$0.0375Bi_{0.5}Na_{0.5}Zr_{0.85}Hf_{0.15}O_3$ (KNNS-BNZH)[13], $(K_{0.5-x}Li_x)Na_{0.5}(Nb_{1-y}Sb_y)O_3$ (KLNNS)[14] and barium titanate $(BaTiO_3)$[15] in order to study their ferroelectric properties (coercive field, impedance, hysteresis loop), their dependence with frequency, besides to gain a deeper insight into the dependance of the dielectric constants with these magnitudes[16]. Likewise, the interest in ferroelectric materials for many technological purposes[17,18] has risen significantly due to their suitability as components of new non-volatile memories (FeRAM)[19−24] aimed to replace gate oxides in future DRAMs[24] or as the gate stack of a transistor (FeFET)[24,25].

Since every ferroelectric is in fact piezoelectric (and pyroelectric[4]), piezoelectric ceramics are a good source of ferroelectric materials to be investigated. Moreover, PZT systems exhibit excellent electrical properties such as very high permittivity and thermal estability with low coercive field[26], and are currently under investigation as capacitors for FeRAM[27]. Additionally, PZT present a high electromechanical coupling coefficient, which means that they can be easily poled and feature a very high Curie Temperature, allowing them to be fully operational across a wide temperature range[28]. In this work we have carried out an in-depth study of ferroelectric behavior, measuring the change in ferro- and piezoelectric properties with temperature. In particular, we focused our study at low temperatures, where previous research is scarce. The devices under study were buzzers whose piezoelectric component was PZT.

II.   FERROELECTRIC POLARIZATION AND PIEZOELECTRIC RESONANCES

In this section, we shall introduce some key concepts which will be useful for interpreting the results of our experiments.

A.   Ferroelectric polarization

A necessary, although not sufficient, microscopical condition for a material to exhibit a spontaneous electric polarization consists in possessing a noncentrosymmetric arrangement of its constituent ions and their corresponding electrons[29]. As we stated in the introduction, in order to be considered as a ferroelectric, the electric polarization of the material must be switchable, and so a nonreconstructive transition between two metastable states of opposite polarization must be accessible at certain electric fields[4]. Similarly to the case of ferromagnet-

ics, several physically relevant magnitudes arise from the existence of hysteresis loops of $P-E$, such as the coercive field E_c, the remnant and saturation polarizations (P_r and P_s respectively), and the dielectric loss of the sample (equal to the area enclosed within the $P-E$ loop[30]). It has been proved experimentally that these quantities suffer notorious alterations when the temperature of the ferroelectric is changed, no matter whether these were PZT thin films[31,32] or other ferroelectrics[30,33].

Ferroelectric crystals exhibit regions where the electric polarization is aligned accordingly so as to minimize their global electrostatic energy[34]; the set of poled loci constitutes their domain structure. Due to the finite size of the domains, it is expected that the overall balance of the minimized energy should contain terms with the opposite dependence on the width of the domain[35]; in the case of ferroelectrics, these terms are the energy of the depolarizing field of bound charges of spontaneous polarization on the surface of the crystal and correlation energy or the energy of domain boundaries[35]. Their minimisation for the 180º (laminated) domain structure, results in the so-called Kittle domain structure[35]. Additionally, other non-180º configurations are also possible whenever they contribute to the reduction of the electrostatic energy. Nevertheless, non-180º domain wall motion in thin (thickness less than few microns) PZT films is negligible[31].

Previous studies[31,32] showed that ferroelectric properties of PZT systems are associated with the domain configuration and domain wall motions. For example, the contributions to dielectric and piezoelectric properties can be separated into intrinsic and extrinsic types, which originate from single domain and domain wall motions, respectively[31]. The experimental evidence also suggests that when an electric field is applied to a ferroelectric material, polarization switching occurs through nucleation of domains and the movement of domain walls, which subsequently expand and grow at the expense of the existing domains[36−40]. This movement is a thermally activated process[31]; hence, the variation of the temperature induces a notorious impact on other related magnitudes. The increase in the coercive field in PZT samples as the temperature decreases is due to the fact that domain wall mobility diminishes at low temperatures[31,32]. Furthermore, the temperature dependence of the coercive field indicates that domain reversal in PZT becomes more difficult as the temperature decreases, and so, larger electric fields are required to accomplish it[31].

If we completely polarize a ferroelectric material, i.e., we force its macroscopic polarization to reach the saturation point P_s for a certain thermal conditions and, next, we remove the external electric field, the polarization of the material diminishes to the point of its remnant value P_r. This phenomenon, known as polarization backswitching, represents the energetic instability of the

alignment of domain polarizations in absence of an external driving force (an electric field). Its value is usually computed as[41]: $P_{bc} = P_s - P_r$. Interestingly enough, Wen et al.[33] showed that the dependence between polarization backswitching of PZT and temperature obeys an Arrhenius law between 300 and 433 K[33], increasing with the rise of temperature.

B.   Resonances and temperature dependance models

Classical Mechanics established the physical principle behind resonances: when an external force drives a freely oscillating system around certain frequencies, the oscillations reach a maximum of amplitude. For piezoelectric materials, since there exists an electromechanical coupling, applying an oscillating AC voltage across the device induces resonant behavior at certain certain frequency(ies) f without the need for mechanical stimulation[46]. On the other hand, there exist manifestations of the opposite kind as well, i.e., frequency(ies) at which the amplitude drops significantly; they are called anti-resonances and, in the case of piezoelectric materials, are located always at higher frequencies nearby resonances.

The sample response to different applied signals can be measured externally by acoustic means – for instance, characterising the sound pressure level as a function of the frequency – and by means of electrical impedance Z_E. Given the previous experimental results[46], we expected to find resonances at impedance minima since this magnitude is an indicator of current flow or charge generation; parallel, anti-resonances were expected to appear at impedance maxima. Additionally, since Z_E is a complex magnitude, the behavior of the phase must also be examined. So far, a good number of electromechanical models[47] have been proposed along the years to relate both the electrical and mechanical impedances. A pioneering study conducted by Liang et al.[48] concluded that the electrical impedance of the PZT patch, after a one dimensional assumption, can be written mathematically as:

$$Z_E(\omega) = \frac{1}{j\omega a}\left(\epsilon_{33}^T - \frac{Z_S(\omega)d_{31}^2}{s_{11}^E(Z_E(\omega) + Z_P(\omega))}\right)^{-1} \quad (1)$$

where $\omega = 2\pi f$, $Z_P(\omega)$ and $Z_S(\omega)$ are the mechanical impedance of the PZT patch and the monitored structure, respectively; a is a geometric constant that depends on the shape and size of the patch; j is the unit imaginary number; and ϵ_{33}^T, d_{31} and s_{11}^E are the dielectric constant at constant stress, the axial piezoelectric coefficient, and the elastic compliance at constant electric field respectively (considering the one-dimensional assumption[48]). The piezoelectric coefficients represent the change in volume of the material when an electric field is applied through it. It has been shown experimentally that both the axial (d_{31}) and longitudinal (d_{33}) piezoelectric coefficients of PZT ceramics decrease proportionally as the temperature diminishes[49,50]; following Eq. 1, an increment in Z_E with decreasing temperature is naively expected. Nevertheless, piezoelectricity is sensitive to the frequency of the applied voltage as well. Fernandes et al.[52] and Damjanovic[53,54] successfully characterized the temperature and frequency dependence of both d_{31} and d_{33}, which was found to be inversely proportional to the frequency of the applied voltage (equivalently $\omega = 2\pi f$). They also found that these coefficients are directly proportional to the amplitude of the applied electric field, the size of the sample and the temperature. On the other hand, little has been said so far about physically relevant magnitudes such as Z_E or the capacitance. Based on the previously mentioned characterization of piezoelectric coefficients, we expected to register a modification of both the electrical impedance and the resonant conditions across the range of temperatures and frequencies that we planned to expose our PZT devices to.

III.   EXPERIMENTAL SETUP

A.   Piezoelectric diaphragm models

The devices under investigation were piezoelectric diaphragms (buzzers) manufactured by MuRata Manufacturing Co., Ltd. Measurements were carried for the models 7BB-12-9 and 7BB-20-6. The active element in these buzzers is not given by the manufacturer, but, as it was demonstrated by Silva de Freitas et al.[10,11], the ceramic used is PZT, very common for its good behavior as both ferro- and piezoelectric. The dimensions and properties of the buzzers given by the manufacturers are presented in both Fig. 1 and Table 1.
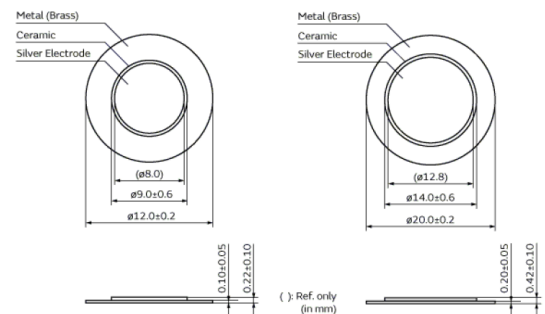

FIG. 1: Schematics of the 7BB-12-9 (left) and 7BB-20-6 (right) piezoelectric diaphragms manufactured by Mu-Rata.

Feature	7BB-12-9	7BB-20-6
Resonance(kHz)	9	6.3
Resonant freq. tolerance(kHz)	±1	±0.6
Resonant impedance(Ω)	1000	350
Capacitance(nF)	8	10
Capacitance tolerance	±30%	±30%
Meas. Condition of Capacitance(kHz)	1	1
Operating Temperature Range($^{\underline{o}}$C)	-20 to 70	-20 to 70
Storage Temperature Range($^{\underline{o}}$C)	-30 to 80	-30 to 80
Shape	No lead wire	No lead wire
Plate Size(mm)	12 ± 0.2	20 ± 0.2
Element Size(mm)	9 ± 0.6	14 ± 0.6
Plate Material	Brass	Brass
Drive Type	External Drive	External Drive
EIAJ Part Number	PD-SU2-C12-90	PD-SU2-C20-63

TABLE I: Dimensions and properties of the 7BB-12-9 and 7BB-20-6 piezoelectric diaphragms manufactured by MuRata.

B. Sawyer-Tower

The electrical characterization of the buzzers was performed using a Sawyer-Tower (S-T) circuit[55] presented in Fig. 2. This technique stands as a common procedure[4,56] for measuring the hysteresis loops of ferroelectric materials. The S-T circuit consists of a capacitance bridge composed of two capacitors, one being the Device Under Test (DUT), in this case the buzzer, and the sensor capacitance (C) consisting of a capacitor of a previously-known value which must be two or three orders of magnitude larger than the sample's so as to ensure that the voltage drop across the sensor capacitance is far less than that across the sample, forcing the voltage in C to give the polarization of the DUT. In our measurements, C = 10 μF (three orders of magnitude larger than the DUT capacitance).
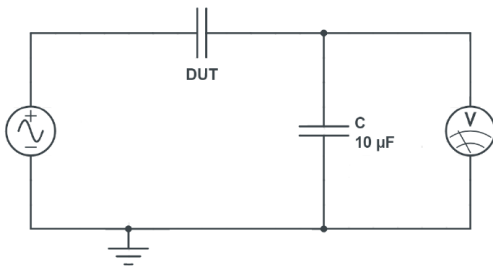

FIG. 2: Schematic representation of the Sawyer-Tower circuit.

To obtain the IV curves for our buzzer, a voltage ramp was applied until the PZT was completely polarized, and then the same ramp was applied with the opposite sign, thus performing a double sweep which delivered a bi-

valued function. Shortly afterwards, we measured two current values for each voltage applied (both positive and negative) that corresponded to the sample being polarized or not. The hysteresis loop, commonly presented in the literature as a Polarization-Voltage (P-V) loop, will be featured in the following pages as a Charge-Voltage (Q-V) graph; the charge values were calculated integrating the current values acquired in the DUT.

C. Voltage divider

To analyze the buzzers impedance response, we used a voltage divider as seen in Fig. 3 and applied a frequency sweep ranging from 5 kHz to 20 kHz using a sinusoidal wave (provided by *Keysight 33250A*). R refers to the internal impedance of the oscilloscope (*Agilent DSO-X 3104A*), set at 50 Ω for this purpose.

It is easy to compute the dividers' transfer function:

$$\frac{V_{in}}{V_{out}} = \frac{IR}{I(Z+R)} = \frac{R+Z}{Z} = 1 + \frac{Z}{R} \qquad (2)$$

Providing the definition $Z = X + jY$ and de Moivre formula, we can express the Real (X) and imaginary (Y) parts of the impedance (Z) in terms of the argument (φ) and module $M = \frac{V_{in}}{V_{out}}$:

$$M\cos(\varphi) = 1 + \frac{X}{R} \quad M\sin(\varphi) = \frac{Y}{R} \qquad (3)$$

The oscilloscope performed measurements of V_{in}, V_{out} and φ, understanding de latter as the *phase* shift between the *in* and *out* waves. With this data, we were able to calculate X, Y, and thus, Z:

$$X = R \cdot (M\cos(\varphi) - 1) \qquad (4)$$

$$Y = M \sin(\varphi) \cdot R \qquad (5)$$

$$Z = \sqrt{X^2 + Y^2} \qquad (6)$$

Temperature dependence experiments were performed following the steps mentioned above. The sample was placed in a liquid nitrogen cryostat (*Cryostat DN*) controlled by a thermostat (*Oxford Instruments ITC 502*), where measurements were carried out from 100 K to 320 K.
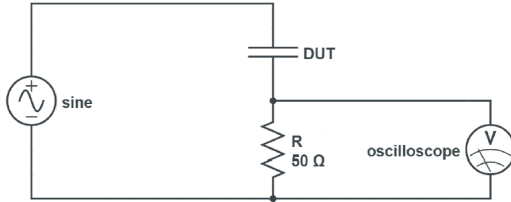
FIG. 3: Schematic representation of the Voltage Divider circuit.

IV.   CHARACTERIZATION RESULTS AND DISCUSSION

A.   Polarization hysteresis

As for the polarization of the 7BB-12-9 model, our goal was to obtain the polarization curve for positive and negative voltages; applying a voltage ramp from 0 to 300 V guaranteed the visualization of the entire curve at room temperature (300 K). The IV curve and hysteresis loop (Fig. 4) confirmed that the ceramic used in the buzzers showed an excellent ferroelectric behavior.

Afterwards, the sample was introduced into the cryostat and we performed the same measurements across different temperatures: from 100 to 320 K with a step of 10K. As we shall further address in this paper, the acquisition of the curves for all thermal conditions required an increase in the maximum value of the voltage ramp up to 500 V, with no reported impact in the integrity of the sample.

The growth of the coercive field means that the temperature of the sample significantly influences on the dielectric response at a given electric field: cooling the ceramic caused the gradual loss of its identitarian hysteresis loop[57], transforming into the typical curve of a lossy dielectric[58]. This issue can also be addressed regarding the growth of the dielectric losses of the PZT buzzer (the area enclosed by the Q-E loop), and our evidence is supported by several previous papers[30,33,59].
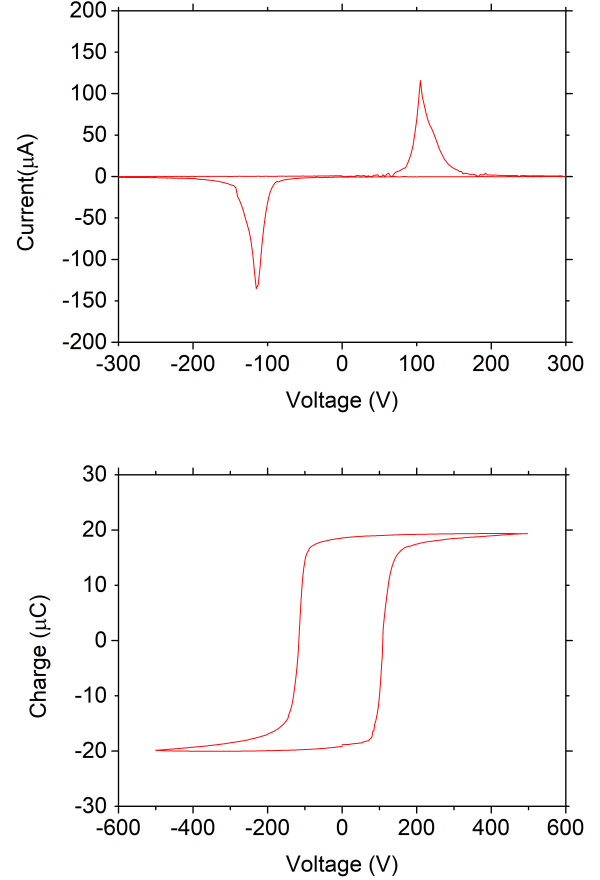

FIG. 4: **Top -** IV curve of the 7BB-12-9 MuRata buzzer at 300 K. **Bottom -** Hysteresis loop of the same buzzer at the same thermal conditions.
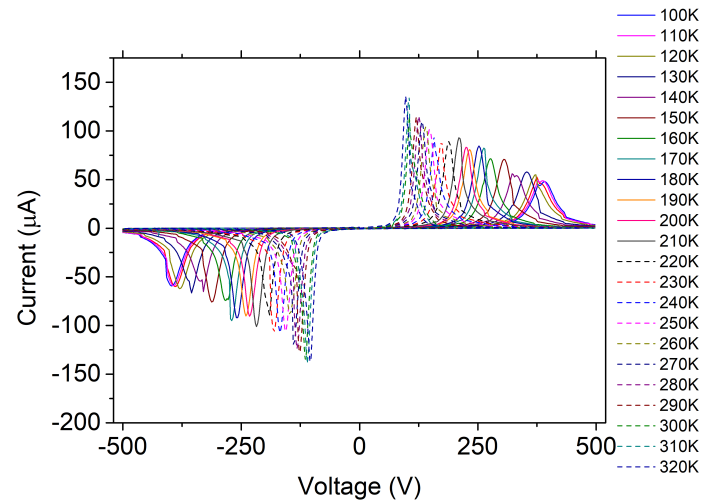

FIG. 5: IV polarization curves of the 7BB-12-9 for each temperature in the range 100-320 K.

5

While observing the IV curves for each temperature in Fig. 5, we noticed that the lower the temperature of the sample, the higher the voltage needed in order to fully polarize the ceramic. Moreover, the current peak obtained by the polarization process dropped smoothly as the sample got colder. This suggested us that the lower the temperature of the sample, the weaker the activation of the inverse piezoelectric effect, and thus, a higher electric field is needed to polarize the sample. This behavior can be explained regarding ferroelectric polarization as a consequence of domain wall motion, a thermally activated process[31]. Consequently, as temperature decreases, domain reversal becomes gradually tougher; therefore, the electric fields needed to polarize the sample are larger. In addition, the polarization currents decrease, which could be attributed to the inability to reverse all the domains at such low temperatures. The fact that domain walls lose mobility and cannot be all reversed as the temperature lowers explains the increase of the coercive field with the drop of temperatures[32]. Fig. 6 presents a 3D plot (Q-V-T) of the hysteresis loop where the rise of the coercive field with temperature is noticeable (since E and V are proportional to each other). Moreover, the "gap" between both the first and the last charge values in the hysteresis loops are explained due to different polarization states at the beginning and the end of the experiment.
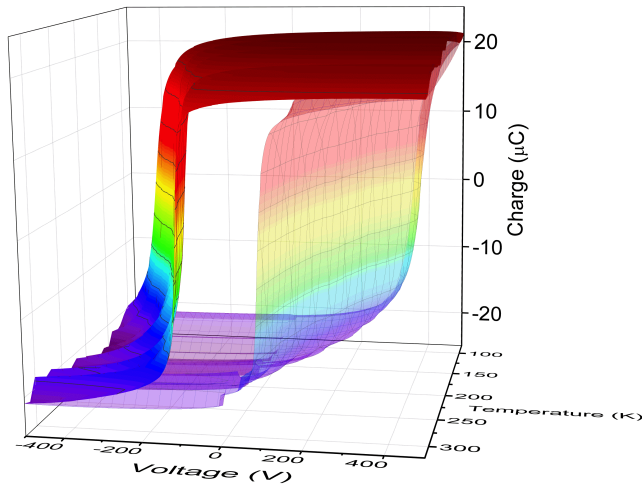

FIG. 7: IV polarization curves of the 7BB-20-6 for each temperature in the range 100-320 K.

FIG. 6: Variation of the 7BB-12-9 buzzer's hysteresis loop with temperature. Warmer (cooler) colours indicate higher (lower) charge values.

FIG. 8: **Top** - IV curve of the 7BB-12-9 (red) and 7BB-20-6 (black) piezoelectric diaphragms at 300 K. **Bottom** - Hysteresis cycle of the 7BB-12-9 (red) and 7BB-20-6 (black) piezoelectric diaphragms at 300 K.

B.   Size dependence

In order to characterize another buzzer from the same manufacturer, and to measure possible size dependences, the same experiments described above were carried for a
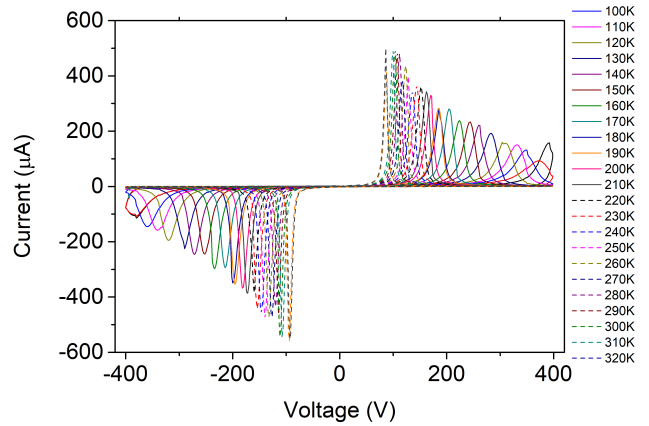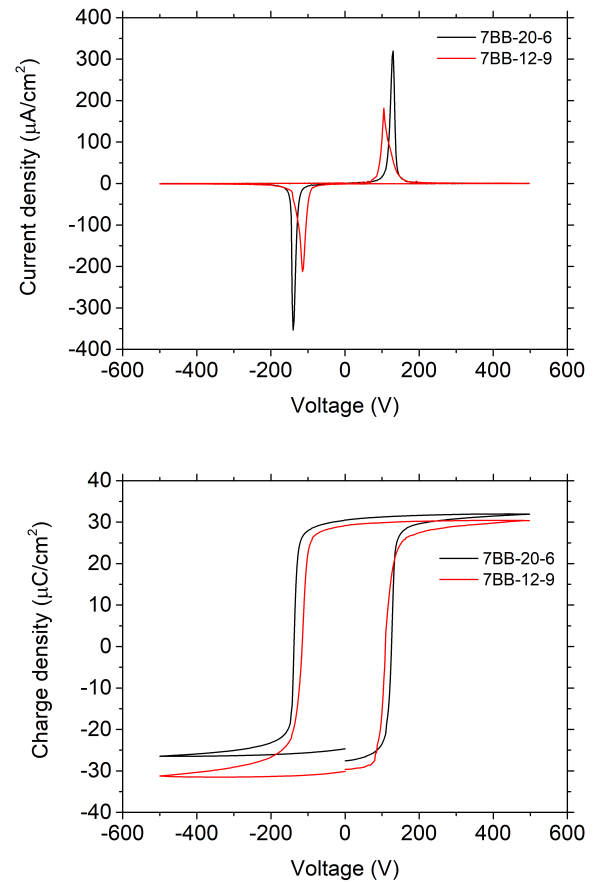
new diaphragm model 7BB-20-6. The temperature sweep (Fig. 7) showed that the behavior of the current peaks followed the same pattern observed in the first sample (Fig. 5), although they are noticeably higher, meaning that this new diaphragm stores a larger quantity of polarized charge (keep in mind that this new diaphragm is significantly larger than the previous one, as presented in Table 1). Likewise, Fig. 8 presents the normalized comparison (using densities instead of absolute magnitudes) between the IV polarization curve and the $Q - E$ loops of both samples. The top graph shows that, at 300 K, the peak corresponding to the current density of the 7BB-20-6 model almost doubles the height of that of the 7BB-12-9, whereas the bottom graph presents a narrow difference between the charge density of both buzzers. Taking a closer look at the current peaks will persuade the reader that the 7BB-20-6 peak is narrower than the 7BB-12-9 peak. This suggested us that the domain size distribution is more even in the largest buzzer than in the smallest, despite producing the same charge density.
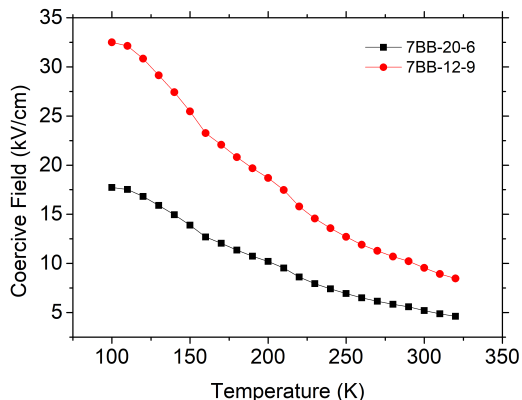

FIG. 9: Coercive field of the 7BB-12-9 (red) and 7BB-20-6 (black) piezoelectric diaphragms in the 100–320 K temperature range.

Furthermore, we measured the relationship between the magnitude of the coercive field and temperature corresponding to the 7BB-12-9 and 7BB-20-6 models (Fig. 9). Similar behavior had been found previously by Xu et al.[31] and Meng et al.[32]. The rise of the coercive field as the temperature decreases is due to the fact that domain wall motion is thermally activated; hence, as the temperature lowers, the inability to reverse all domain walls combines with the reduced mobility of the reversible ones, some of them even pin[31], leaving, as a result, the need for more intense electric field values and the decrease in the poling currents). Even though this behavior is common for both samples, we cannot ignore that, in fact, there IS a dependence in the poling processes of the samples regarding their size which becomes even more pronounced at lower temperatures. It has been reported that the size

of the sample affects the poling process as well[31,32]; in our case, the smaller the diaphragm, the lesser mobility of the polarization domain walls and the more poling from nucleation, causing the coercive field to rise as seen in Fig. 9. Following the findings presented by the previous authors[31,32], Fig. 9 also suggests that the crystalline grains of the 7BB-20-6 sample are significantly thinner than those of the 7BB-12-9 sample.

The phenomenon of polarization backswitching opposes the polarization switching we explained before (the nucleation and mobility of domain walls) and affects the sample notoriously when the external electric field is removed[33], acting as a driving force against the alignment of the polarization domains. Fig. 10 presents the logaritmic plot of the measured relationship between the polarization backswitching and the inverse temperature of the two buzzers, agreeing with the fact that this phenomenon intensifies at higher temperatures found by Wen et al.[33] in both cases. On the other hand, our data expands the knowledge of this phenomenon and confirms that it follows an Arrhenius-like behavior only for temperatures higher than a certain threshold ($\sim$ 150 K for the 7BB-12-9 and $\sim$ 120 K for the 7BB-20-6). We believe that this issue is closely related to the different size of the crystalline grains between both samples pointed out by the coercive field dependence. The grains of the smallest ceramic buzzer are more difficult to polarize than those of the other one (in other words, domain wall motion is tougher), causing the saturated state to be less stable. Consequently, when the force of the external electric field is removed, a larger number of domains return to the unaligned situation in the smallest sample, increasing the difference between the P_s and the P_r states, i.e., polarization backswitching.
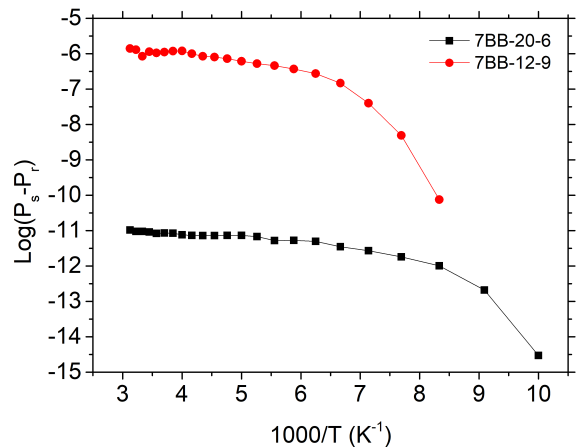

FIG. 10: Logaritmic plot of the evolution of polarization backswitching of the 7BB-12-9 (red) and 7BB-20-6 (black) buzzers with temperature.

C. Impedance analysis

In III C we explained the voltage divider circuit whose known resistor was the impedance of the oscilloscope's channel 2 (set to 50 Ω). Fig. 11 presents the electrical impedance (impedance from now on) at room conditions (300 K) of 7BB-12-9. We identified several resonances at 6 kHz, 12 kHz, 15 kHz and 17.5 kHz besides from the one given by the manufacturer at 9 kHz (the global maximum); in spite of this findings, we believe the two little maxima at 12 kHz and 17.5 kHz may be harmonic frequencies of the first two resonances (the same cannot be said for the 15 kHz peak).

In order to carry out a more careful analysis of these resonances while ensuring the validity of the results we performed a sound level analysis. At room temperature, a sound level meter was placed in front of our piezoelectric diaphragm, and the frequency sweep was carried as previously described. Here (Fig. 12), the sound pressure maxima match properly the resonance peaks observed in Fig. 11. Additionally, we proved that the buzzer possesses fine electroacoustic properties in the human audible frequency range, which would make it suitable for alarms or SHM applications. However, the response between 15 and 17.5 kHz is much significant in comparison with the impedance measurement, and the 12 kHz peak is missing. Although this difference could seem large enough to doubt on the acquired curves, it must be noted that the magnitude whose significant changes compare better with the sound pressure is in fact the phase shift between the *in* and *out* electric waves. We present the phase shift throughout the same frequency sweep in Fig. 13, confirming the results of our impedance calculations.
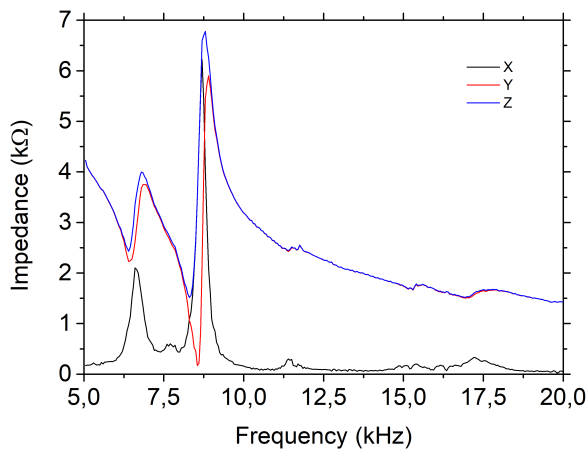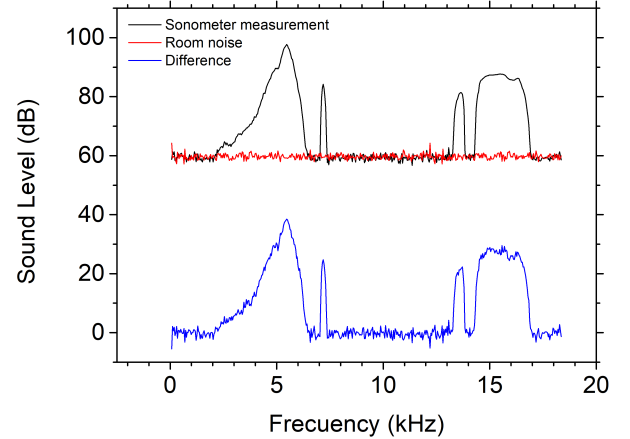

FIG. 12: Sound pressure levels of the 7BB-12-9 MuRata buzzer across the frequency sweep.
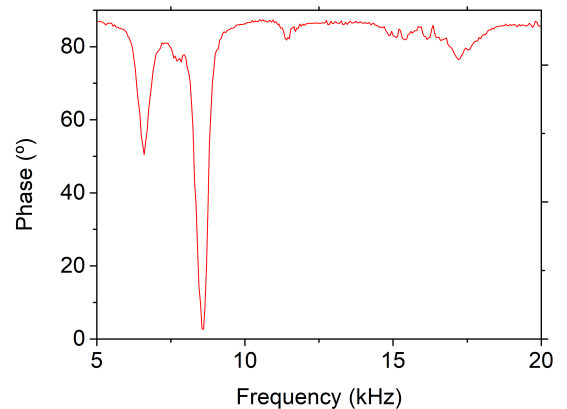

FIG. 13: Phase shift between the *in* and *out* electric waves in the 7BB-12-9 buzzer across the frequency sweep.

Subsequently, the 7BB-12-9 buzzer was placed inside the cryostat in order to carry temperature measurements similarly as above (performing a frequency sweep for each temperature so that we are able to plot a 3D graph of the impedance against both frequency and temperature). The results provided by Fig. 14 indicate that, generally, the anti-resonant peaks grow sharper and higher continuously along the temperature decline and, interestingly, the 6 kHz peak surpasses that of 9 kHz in height. The flattening of the sharp impedance peaks with growing temperature recorded in Fig. 14 has been observed in a previous work by G. Park et al[60]. Following their reasoning, it was attributed to a decrease in the dynamic interaction between the PZT patch and the two electrodes of the buzzer[60].
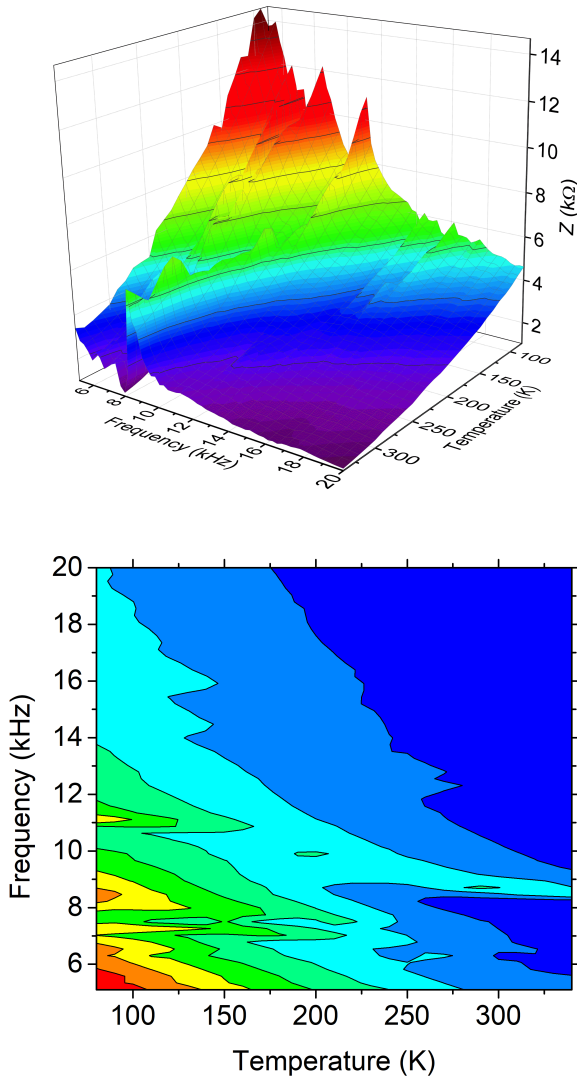

FIG. 11: Impedance (Z) buzzer's response in blue. Both imaginary (Y) and real (X) parts are presented in red and black respectively.

FIG. 14: **Top -** 3D graph of the impedance (Z). **Bottom - ** Contour plot of Z in frequency vs temperature, where the shift towards higher frequencies at lower temperatures can be clearly noticed. Warmer (cooler) colours indicate higher (lower) Z values.

We claim that the fact that the impedance values (especially anti-resonant peaks) rise as temperature decreases can be explained by the inversely squared proportional relationships existing between the impedance and the piezoelectric coefficients (recall Eq. 1). Silva de Freitas et al.[11] proved that the inverse piezoelectric effect is dominated by the piezoelectric coefficients which affect the impedance value[11,48], and depend both on the frequency[53,54] of the electric field and temperature[51]. To investigate what happened to these coefficients (in other words, to the ability of the PZT to change its volume when an external electric field is applied to it), we noticed the shift towards higher frequencies at lower tem-

peratures experienced by the resonances, similar to that recorded by Lim et al. while applying tensile stress to PZT patches[61]. This led us to believe that the temperature change experimented by our buzzer was in fact a source of internal stress inducing an stiffening effect to the piezoelectric ceramic. Consequently, the piezoelectric coefficients reduced their value, resulting in larger values for the impedance (recall the dependence between both magnitudes expressed in Eq. 1[48]). There is only one critical exception: the resonance at 9 kHz, which presents a valley at around 200 K and loses its condition of global maximum to the resonance at 6 kHz. The analysis of the real part (X) confirmed this behavior (Fig. 15).
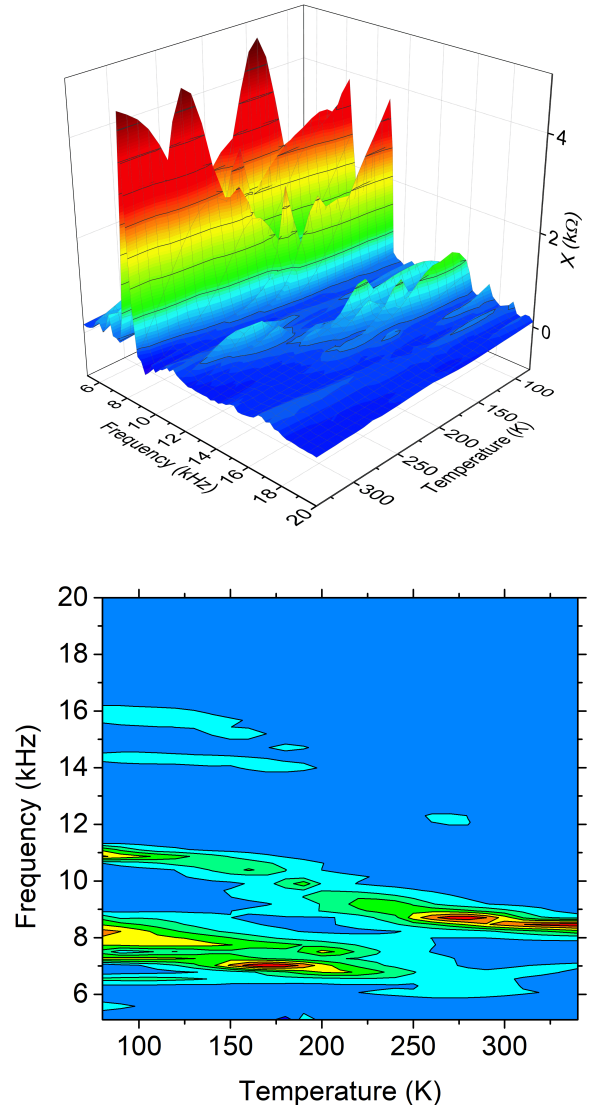

FIG. 15: **Top -** 3D graph of the impedance real part (X). **Bottom -** Contour plot of X in frequency vs temperature, where the valley around 9 kHz can be clearly noticed. Warmer (cooler) colours indicate higher (lower) X values.

9

We believe that this was the result of a trade-off between the temperature and frequency effects on the piezoelectric coefficients values. The lack of previously published research highlighting this issue allows us to open a new researching field aimed at future researchers of this area. Additionally, we characterised the behavior of the electric permittivity ε under the temperature and frequency conditions employed throughout this work due to its relationship with Z via dielectric constant (Eq. 1). First, we computed the values for capacitance of the PZT ceramic, shown in Fig. 13 at 300 K and in Fig. 16, using the following expression:

$$C = \frac{1}{\omega Y} \tag{7}$$

where ω is the angular frequency: $\omega = 2\pi f$. It is clear from Fig. 16 that the only resonance which severely affects the capacitance values is the one at 9 kHz and high temperatures. Once the resonance frequency is exceeded, the capacitance reaches an almost constant value throughout the frequency range, which increases almost unnoticeably with temperature.
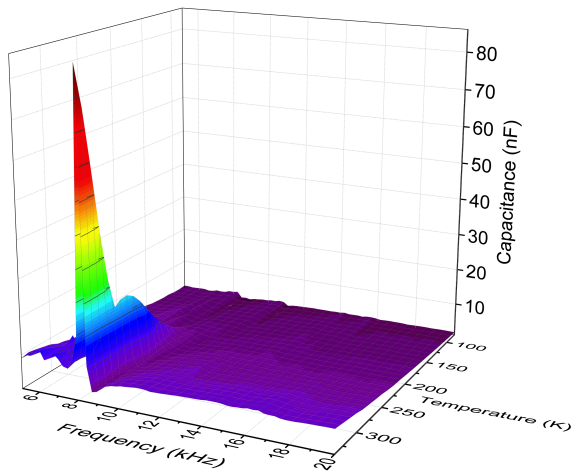

FIG. 16: 3D graph of the capacitance against temperature and frequency. Warmer (cooler) colours indicate higher (lower) capacitance values.

Thanks to our knowledge of the sample's dimensions, we were able to compute the electrical permittivity of the PZT as:

$$\varepsilon = \frac{C \cdot \phi}{A} \tag{8}$$

where A stands for the surface of the buzzer's ceramic and ϕ for the ceramic's thickness . It was interesting to focus on its values along the 10-20 kHz range, where there is no permittivity resonance and the capacitance presents an almost-constant value. Fig. 17 shows that the ε values increase continuously with temperature at different

frequencies (consistent with the results previously presented by Xu et al.[31], Meng et al.[32] and Sabat et al.[50]) and, on the other hand, remain approximately at constant values for each temperature throughout the whole frequency range (the values fluctuate between 5 and 27 $\frac{nF}{m}$, indeed the usual values for PZT ceramics[31,32]).
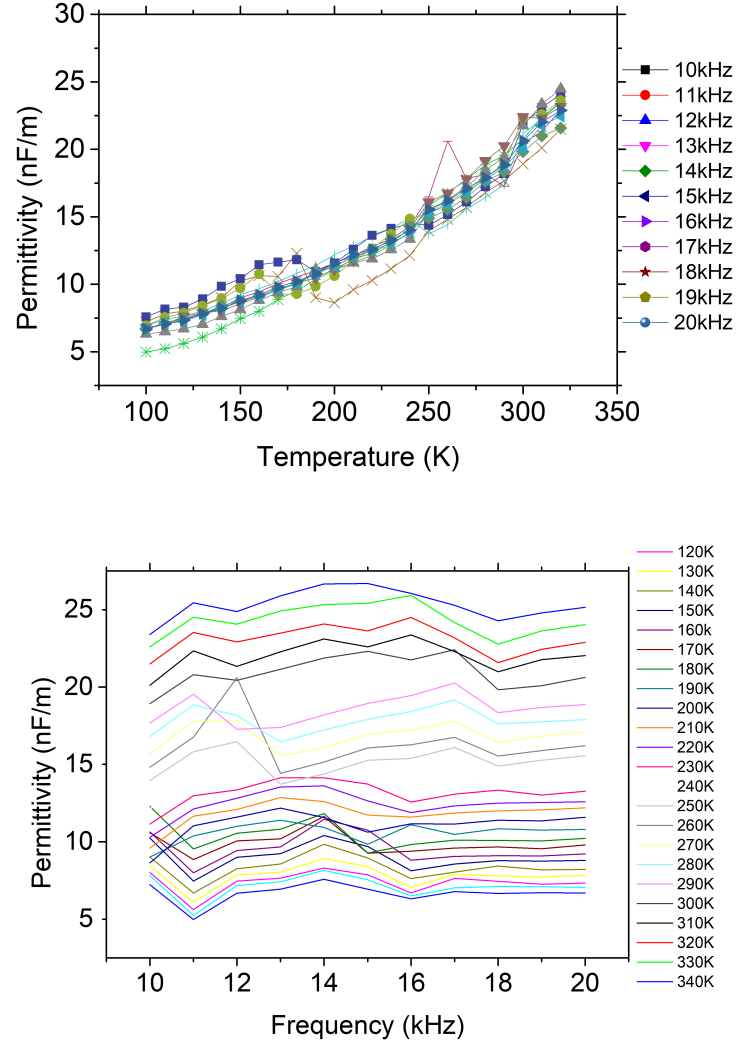

FIG. 17: **Top** - Electrical permittivity in the 100-320 K range. Each curve represented corresponds to a different frequency value in the 10-20 kHz range, with a step of 1 kHz. **Bottom** - Electrical permittivity in the 10-20 kHz range. Each curve represented corresponds to a different temperature value in the 100-320 K range, with a step of 10 K.

V.   CONCLUSIONS

In this work we have carried out an in-depth experimental study of low-cost piezoelectric diaphragms. The electric characterization showed that the buzzers studied exhibited an excellent ferroelectric behavior at high voltages, without repercussions in the samples' integrity. Data extracted from the temperature measurements led us to realize that the samples became more difficult to polarize as the temperature decreased, requiring more voltage and presenting lower polarization currents. This means that reducing the temperature delays the activation of the inverse piezoelectric effect and minimizes its outcome. This behavior could also be noted thanks to the acquisition of hysteresis loops at several temperatures, which indicated that coercive fields grow as temperature drops. Both temperature-related effects can be explained by the fact that polarization switching is driven by domain wall motion, a thermally activated process, and so domain walls have less mobility or are even unable to be reversed when the temperature lowered.

We found evidence to support the existence of size dependence between both diaphragms, highlightened by the differences between their current density, coercive fields and their backswitching polarization. Based on previous evidence, we concluded that the 7BB-12-9 buzzer presents polarization domain walls with less mobility and thicker crystalline grains than its counterpart. Polarization backswitching turned out to exhibit some similar behavior with temperature for both cases, Arrhenius-like up to a certain limit followed by a marked decline not found in previous literature, whilst clear differences in magnitude between both sizes were observed.

Our impedance analysis showed that, besides the main resonance at 9 kHz, the 7BB-12-9 buzzer presents another important resonance at 6 kHz along with some less important resonant phenomena at 12 kHz, 15 kHz and 17.5 kHz, (which aside from the 15 kHz one are probably just harmonic frequencies of the 6 kHz and 9 kHz ones). These results were ratified by a sound level meter detection of similar sound pressure maxima around those of the impedance ones. This measurement proved also the buzzer's perfectly functional electroacoustic properties in the human-hearing range.

The simultaneous frequency and temperature sweep indicated that impedance resonances shifted towards higher frequencies as the sample got cooler, and the impedance grew noticeably as temperature dropped (especially anti-resonance peaks). This last feature was attributed to the inversely proportional relationship between the decreasing piezoelectric coefficients and the impedance as well as the loss of dynamic interaction between the PZT patch and the two electrodes of the buzzer, following previous research. We believe that the shift towards higher frequencies can be explained thanks to the combination of two factors. The first one would be the appearance of an internal stress in the ceramic which generated larger stiffness and, consequently, reduced its piezoelectric coefficients. The second one would be the inversely proportional relationship discovered between the electrical permittivity of the sample and its temperature. Additionally, we found that the 6 kHz anti-resonance emerged at the lowest temperatures as the impedance global maximum. The same behavior was observed for both the imaginary and real parts of the impedance, although for the real part the main resonance at ambient or higher temperatures (9 kHz) presented a valley in the 200 K range of which we have found no previous experimental nor theoretical evidence before becoming the second maximum at lower temperatures. We claim that this behavior was the result of a trade-off between the temperature and frequency effects on the piezoelectric coefficient values, and we would like to make a call to other researchers in order to investigate this phenomenon.

The capacitance presented a huge and solitary maximum at high temperatures on the main resonance (9 kHz), although a slightly decrease in its value could be noted as temperature dropped at frequencies higher than 10 kHz. Since the electrical permittivity is proportional to the capacitance, its behavior remained the same, reaching a value between 5 and 27 $\frac{nF}{m}$ throughout the 10-20 kHz/100-320 K range (ratifying the fact that the ceramic used in the diaphragm is PZT).

VI.   ACKNOWLEDGMENTS

VII.   REFERENCES

[1] P. Curie , and J. Curie. Bulletin de la Société Minérologique de France. **3** (4): pp. 90–93. (1880)
[2] S. Katzir. Notes Rec. R. Soc. **66** (2): 141–157 (2012).
[3] J. Valasek. Physical Review. **15** (6): 537 (1920).
[4] K. M. Rabe, M. Dawber, and C. Lichtensteiger, Springer (2007).
[5] W. Wersing. Ferroelectric Devices. In: Setter N., Colla E.L. (eds) Ferroelectric Ceramics. Monte Verità (Proceedings of the Centro Stefano Franscini, Ascona). Birkhäuser Basel (1993).

[6] J. Krautkrämer, H. Krautkrämer, Ultrasonic Testing of Materials, pp. 119-149 (1983).

[7] H. Hoshyarmanes, and A. Abbasi. Journal of Intelligent Material Systems and Structures, 29(9), pp. 1799–1817 (2018).

[8] H. Hoshyarmanes, N. Ebrahimi, A. Jafari, P. Hoshyarmanesh, M. Kim, and H. Park. Sensors, 19, 13 (2019).

[9] H. Mei, M. F. Haider, R. Joseph, A. Migot and V. Giurgiutiu, Sensors 19, 383, (2019).

[10] E. Silva de Freitas, F. G. Baptista, D. E. Budoya, and B. A. de Castro, IEEE Sensors Journal 17, No. 17 (2017).

[11] E. Silva de Freitas and F. Guimarães Baptista, Sensors and Actuators A 238 pp. 220–228 (2016).

[12] Y. Zhang, Z. Chen, W. Cao, and Z. Zhang, App. Phys. Lett. 111, 172902 (2017).

[13] L. Qiao, G. Li, H. Tao, J. Wu, Z. Xu, and F. Li, Ceramics International 46, Issue 5, pp. 5641-5644 (2020).

[14] L. Wu, D. Xiao, J. Wu, Y. Sun, D. Lin, J. Zhu, P. Yu, Y. Zhuang, and Q. Wei, Journal of the European Ceramic Society 28, pp. 2963–2968 (2008).

[15] S. Singh, B. Singh, S. Kumar, and A. K. Yadav, Ferroelectrics 551, 1, pp. 133-142 (2019).

[16] G. A. Samara, Ferroelectrics 2, 277-289 (1971).

[17] N. Setter, D. Damjanovic, L. Eng, G. Fox, and S. Gevorgian, J. App. Phys. 100, 051606 (2006).

[18] L. W. Martin, Y.H. Chu, and R. Ramesh, Mater. Sci. Eng. R. 68, pp. 89–133 (2010).

[19] S. Meena, S. M. Sze, U. Chand, and T.-Y. Tseng, Nanoscale Research Letters 9, 526 (2014).

[20] O. Auciello, J. F. Scott, and R. Ramesh, Physics Today 51(7), 22 (1998).

[21] S. Hoffmann-Eifert, and T. Watanabem, Chapter 6: FeRAM, Atomic Layer Deposition for Semiconductors, pp. 149-171 (2014).

[22] Wang, L., Yang, C., and Wen, J., Electron. Mater. Lett. 11, pp. 505–543 (2015).

[23] A. Chen, Solid-State Electronics 125, 2pp. 5–38 (2016).

[24] M. Dawber, K. M. Rabe, and J. F. Scott, Rev. Mod. Phys. 77, No. 4, pp. 1083-1130 (2005).

[25] H. Ishiwara, Multifunctional Oxide Heterostructures (2012).

[26] Jaffe, B., Cook, W., and Jaffe, H., Piezoelectric Ceramics. Academic, New York, pp. 185–212 (1971).

[27] G. H. Haertling, J. A. Ceram. Soc. 82 (4), 797-818 (1999).

[28] J. S. Cross, M. Fujiki, M. Tsukada, K. Matsuura, S. Otani, M. Tomotani, Y. Kataoka, Y. Kotaka, and Y. Goto, Integrated Ferroelectrics 25, 1-4, pp. 265-273 (1999).

[29] K. Rabe, C. H. Ahn, J.-M. Triscone (Eds.): Physics of Ferroelectrics: A Modern Perspective, Topics Appl. Physics 105, 175–218 (2007).

[30] J. and G. Chapman et al. Journal of the American Ceramic Society 101 (2017).

[31] F. Xu, S. Trolier-McKinstry, W. Ren, and Baomin Xu. J. App. Phys. 89, 1336 (2001).

[32] X. J. Meng, J. L. Sun, X. G. Wang, T. Lin, J. H. Ma, S. L. Guo, and J. H. Chu, Appl. Phys. Lett. 81, 4035 (2002).

[33] Wen, B., Zhang, Y., Liu, X. et al. J Mater Sci 47, 4299–4304 (2012).

[34] M. Vopsaroiu, J. Blackburn, M. G. Cain, and P. M. Weaver. Physical Review B. 82, 024109 (2010).

[35] A. S. Sidorkin, Domain Structure in Ferroelectrics and Related Materials, Cambridge Int Science Publishing, 1-25 (2006).

[36] W. J. Merz, Phys. Rev. 95, 690 (1954).

[37] D. Berlincourt, and H. H. A. Krueger, Journal of Applied Physics 30, 1804 (1959).

[38] Dragan Damjanovic, Rep. Prog. Phys. 61, 1267 (1998).

[39] Rolf Landauer, Journal of Applied Physics 28, 227 (1957).

[40] L. Tian, David A. Scrymgeour, and Venkatraman Gopalan, Journal of Applied Physics 97, 114111 (2005).

[41] Y. Zhang, X. L. Zhong, Z. H. Chen, J. B. Wang, and Y. C. Zhou, Journal of Applied Physics 110, 014102 (2011).

[42] S. Hashimoto, H. Orihara, and Y. Ishibashi, J. Phys. Soc. Jpn. 63, 1601 (1994).

[43] H. Orihara, S. Hashimoto, and Y. Ishibashi, J. Phys. Soc. Jpn. 63, 1031 (1994).

[44] M. Avrami, J. Chem. Phys. 8, 212 1940.

[45] V. Shur, E. Rumyantsev, and S. Makarov, J. Appl. Phys. 84, 445 (1998).

[46] M. Stewart, M. G. Cain and P. Weaver: Characterisation of Ferroelectric Bulk Materials and Thin Films, Springer, pp. 15-36 (2014).

[47] V.G.M. Annamdas, K.K. Annamdas, Proceedings of SPIE 7292, Sensors and Smart Structures Technologies for Civil, Mechanical, and Aerospace Systems, San Diego, California, USA, 2009, pp. 1–12

[48] C. Liang, F.P. Sun, C.A. Rogers, J. Intell. Mater. Syst. Struct. 5 (1994) 12–20.

[49] R. A. Wolf, and S. Trolier-McKinstry, J. Appl. Phys., Vol. 95, No. 3, 2004.

[50] Sabat, Ribal & Mukherjee, B.K. & Ren, Wei & Yang, Guomao. Journal of App. Phys. 101 064111 (2007).

[51] Q. M. Zhang, H. Wang, N. Kim, and L. E. Cross., J. App. Phys. 75, 454 (1994).

[52] J. R. Fernandes, F. A. de Sá, J. L. Santos, E. Joanni, Review of scientific instruments, Vol. 73, No. 5, 2002.

[53] D. Damjanovic, Phys. Rev. B 55, R649(R) (1997).

[54] D. Damjanovic, J. App. Phys. 82, 1788 (1997).

[55] Sawyer, C.B., and Tower, C.H., Phys. Rev. 35, 269 (1930)

[56] R. Andika, La Ode H. Z. Toresano, M. Hikam, B. Soegijono and A. Sudarmaji, 7th International Conference on Physics and Its Applications 2014 (ICOPIA 2014), Published by Atlantis Press (2015).

[57] J. F. Scott, J. Phys.: Condens. Matter 20, 2, 021001 (2007).

[58] D.A. Hall, NPL, 18th March 1998.

[59] Y. Wang, and J. Wang. Journal of Appl. Phys. 106 094106 (2009).

[60] G. Park, K. Kabeya, H. H. Cudney, D. J. Inman, JSME International Journal, series A, Vol. 42, No. 2 (1999).

[61] Yee Yan Lim, and Chee Kiong Soh. Journal of Intelligent Material Systems and Structures 23 7 (2012).

VIII.   SUPPLEMENTARY INFORMATION

The MATLAB codes used to control both the oscilloscope and the function generator during the polarization (Sawyer-Tower) and impedance (Voltage divider) measurements are presented in the following pages:

Sawyer-Tower:

```matlab
1  clear all;
2  %% Instrument Connection
3  % Find a VISA-GPIB object.
4  ELECTRO = instrfind('Type', 'visa-gpib', 'RsrcName', ...
       'GPIB0::8::INSTR', 'Tag', '');
5  % Create the VISA-GPIB object if it does not exist
6  % otherwise use the object that was found.
7  if isempty(ELECTRO)
8  ELECTRO = visa('AGILENT', 'GPIB0::8::INSTR');
9  else
10 fclose(ELECTRO);
11 ELECTRO = ELECTRO(1);
12 end
13 % Connect to instrument object, obj1.
14 fopen(ELECTRO);
15 figure ('Name','Medidas de ferroelectricidad' );
16 %% parametros de medida
17 % Communicating with instrument object, obj1.
18 numero_ciclos=1;
19 ciclo_inicial=1;
20 vipos = 0;
21 vfpos= 500;
22 vineg = 0;
23 vfneg= -500;
24 pasospos = 200;
25 pasosneg = 200;
26 %RANGO DE CORRIENTE
27 Rango=2e-3;
28 fprintf(ELECTRO, ':INP ON');
29 fprintf(ELECTRO, ':SENS:CURR:RANG %e',Rango);
30 fprintf(ELECTRO,':SOUR:VOLT:RANG 1000')
31 % TIEMPO ENTRE MEDIDAS
32 time= 1e-4;
33 fprintf(ELECTRO, ':SENS:CURR:APER %e',time);
34 %salida de datos
35 directorio= 'd:\pelayo\febrero2020\21febrero';
36 etiqueta='muestra6peque_330K_repeat';
37 %% BUCLE DE MEDIDAS POSITIVAS
38 for ciclo=ciclo_inicial:numero_ciclos+ciclo_inicial-1
39 %%En el lado positivo
40 Q = 0;
41 tic
42 fprintf(ELECTRO, ':OUTP OFF');
43 fprintf(ELECTRO,':SOUR:VOLT:RANG 1000')
44 fprintf(ELECTRO, ':OUTP ON');
45 Vmax=abs(vfpos);
46 interpos = (vfpos-vipos)/pasospos;
47 vi=vipos;
48 vf=vfpos;
49 disp(ciclo)
50 inter=interpos;
51 fprintf(ELECTRO,':SOUR:VOLT:RANG 1000')
52 for i = 1:pasospos
53     V=vi+(i-1)*inter;
```

```matlab
54        time(i)=toc;
55        fprintf(ELECTRO, ':SOUR:VOLT %e',V)
56        corriente = str2double(query(ELECTRO, ':MEAS:CURR?'));
57        if i==1
58            carga(i) = Q + time(i)*corriente;
59        else
60            carga(i) = Q + (time(i)-time(i-1))*corriente;
61            Q =carga (i);
62    end
63    VG(i)=V;
64    IG(i)= corriente;
65    absIG(i)=abs(corriente);
66    % figure (2);
67    % subplot (2,1,1)
68    % plot (VG,carga,'m');title ('Q-V Cycle'); xlabel ('VG ...
           (V)');ylabel ('Q (C)');
69    % grid on; hold on;
70    % subplot (2,1,2)
71    % plot (VG,IG,'m');title ('I-V Cycle'); xlabel ('VG (V)');ylabel ...
           ('IG (A)');
72    % grid on;
73    % hold on;
74    end
75    for i = pasospos+1:2*pasospos
76        V=vf+(pasospos-i)*inter;
77        time (i) = toc;
78        fprintf(ELECTRO, ':SOUR:VOLT %e',V);
79        corriente = str2double(query(ELECTRO, ':MEAS:CURR?'));
80        if i==1
81            carga(i) = Q + 1e-3*corriente;
82        else
83            carga(i) = Q + (time(i)-time(i-1))*corriente;
84            Q =carga (i);
85    end
86    Qpos=Q;
87    VG(i)=V;
88    IG(i)= corriente;
89    absIG(i)=abs(corriente);
90    % figure ('Name', 'Lazo IV');
91    % subplot (2,1,1)
92    % plot (VG,carga,'m');title ('Q-V Cycle'); xlabel ('VG ...
           (V)');ylabel ('Q (C)');
93    % grid on; hold on;
94    % subplot (2,1,2)
95    % plot (VG,IG,'m');title ('I-V Cycle'); xlabel ('VG (V)');ylabel ...
           ('IG (A)');
96    % grid on; hold on;
97    end
98    %% BUCLE DE MEDIDAS EN NEGATIVO
99    %en el lado de tensiones negativas
100   fprintf(ELECTRO, ':OUTP OFF');
101   fprintf(ELECTRO,':SOUR:VOLT:RANG -1000');
102   fprintf(ELECTRO, ':OUTP ON');
103   interneg = (vfneg-vineg)/pasosneg;
104   vi=vineg;
105   vf=vfneg;
106   inter=interneg;
```

```matlab
107  for i = 1:pasosneg
108      V=vi+i*interneg;
109      j=i+2*pasospos;
110      time (j) = toc;
111      fprintf(ELECTRO, ':SOUR:VOLT %e',V);
112      corriente = str2double(query(ELECTRO, ':MEAS:CURR?'));
113      carga(j) = Q + (time(j)-time(j-1))*corriente;
114      Q =carga (j);
115      VG(j)=V;
116      IG(j)= corriente;
117      absIG(j)=abs(corriente);
118  % figure (2);
119  %
120  % subplot (2,1,1)
121  % plot (VG,carga,'m');title ('Q-V Cycle'); xlabel ('VG ...
         (V)');ylabel ('Q (C)');
122  % grid on;
123  % subplot (2,1,2)
124  % plot (VG,IG,'m');title ('I-V Cycle'); xlabel ('VG (V)');ylabel ...
         ('IG (A)');
125  % grid on;
126      end
127  for i = pasosneg+1:2*pasosneg
128      j=i+2*pasospos;
129      V=vf+(pasosneg-i)*interneg;
130      time (j) = toc;
131      fprintf(ELECTRO, ':SOUR:VOLT %e',V);
132      corriente = str2double(query(ELECTRO, ':MEAS:CURR?'));
133      carga(j) = Q + (time(j)-time(j-1))*corriente;
134      Q =carga (j);
135      VG(j)=V;
136      IG(j)= corriente;
137      absIG(j)=abs(corriente);
138  end
139  Qneg=Q;
140  qoffset = (Qpos-Qneg)/2
141  totalpasos = 2*(pasosneg+pasospos);
142  %% CALCULO DE LA CARGA
143  for i = 1: totalpasos
144      cargacorregida(i) = carga(i) - qoffset;
145  end
146  %% REPRESENTACION GRAFICA
147  subplot (1,2,1)
148  plot (VG,cargacorregida,'r');title ('Q-V Cycle'); xlabel ('VG ...
         (V)');ylabel ('Q (C)');
149  grid on; hold on;
150  subplot (1,2,2)
151  plot (VG,IG,'b-o');title ('I-V Cycle'); xlabel ('VG ...
         (V)');ylabel ('IG (A)');
152  grid on;hold on;
153  %% GENERACION DE FICHEROS DE DATOS
154  %
155  y = [VG; cargacorregida; IG];
156  fid1 = [directorio '\' etiqueta 'ciclo' num2str(ciclo) '.txt'];
157  figura = [directorio '\' etiqueta 'ciclo' num2str(ciclo) '.png'];
158  saveas(gcf,figura)
159  file1 = fopen(fid1,'wt');
```

```matlab
160  fprintf(file1,'%e %e %e \n',y);
161  fclose(file1);
162  %
163  end
164  clear;
```

Divisor de tensión:

```matlab
1   %
2   % Limpiamos variables, cerramos figuras, todo
3   %
4   clear all
5   close all
6   %
7   %% LLAMAR GENERADOR
8   %
9   % Encontramos el generador de onda.
10  %
11  GEN = instrfind('Type', 'gpib', 'BoardIndex', 7, ...
        'PrimaryAddress', 10, 'Tag', '');
12  %
13  % Crear el objeto VISA—GPIB si no existe,
14  % si existe, usa el objeto encontrado.
15  %
16  if isempty(GEN)
17      GEN = gpib('AGILENT', 7, 10);
18  else
19      fclose(GEN);
20      GEN = GEN(1);
21  end
22  %
23  % Nos conectamos con el generador
24  %
25  fopen(GEN);
26  %
27  %% LLAMAR OSCILOSCOPIO
28  %
29  % Encontramos el osciloscopio.
30  %
31  OSC = instrfind('Type', 'visa—usb', 'RsrcName', ...
        'USB0::0x0957::0x17A0::MY53280112::0::INSTR', 'Tag', '');
32  %
33  % Crear el objeto VISA—GPIB si no existe,
34  % si existe, usa el objeto encontrado.
35  %
36  if isempty(OSC)
37  OSC = visa('AGILENT', 'USB0::0x0957::0x17A0::MY53280112::0::INSTR');
38  else
39  fclose(OSC);
40  OSC = OSC(1);
41  end
42  %
43  % Nos conectamos con el osciloscopio.
44  %
```

```
45  fopen(OSC);
46  %
47  %% DEFINICIN VARIABLES
48  %
49  frequencyStart = 5E+3;
50  %
51  frequencyEnd = 15E+3;
52  %
53  paso=5E+1;
54  %
55  numpasos = (frequencyEnd—frequencyStart)/paso;
56  %
57  R = 50;
58  %
59  % Inicializamos los arrays como vectores cero
60  %
61  frequencies = zeros(1, numpasos);
62  V1 = zeros(1, numpasos);
63  V2 = zeros(1, numpasos);
64  f = zeros(1, numpasos);
65  arg = zeros(1, numpasos);
66  %
67  % La impedancia es compleja Z = X + jY
68  %
69  X = zeros(1, numpasos);
70  Y = zeros(1, numpasos);
71  Z = zeros(1, numpasos);
72  %
73  % salida de datos
74  %
75  directorio= 'd:\pelayo\febrero2020\27febrero2020\';
76  etiqueta='Test_rangoT_inverso_80K';
77  %
78  %% DEFINICIN FUNCION DE ONDA
79  %
80  fprintf(GEN,'FUNC SIN');
81  %
82  fprintf(GEN,'FREQ %d', frequencyStart);
83  %
84  fprintf(GEN,'VOLT 20');
85  %
86  fprintf(GEN,'VOLT:OFFS 0');
87  %
88  %% CONFIGURACIN TRIGGER Y OUTPUT
89  %
90  fprintf(GEN,'TRIG:SOUR BUS');
91  %
92  fprintf(GEN, 'OUTPUT ON');
93  %
94  fprintf(GEN,'*TRG');
95  %
96  % Alta Impedancia para el generador
97  %
98  fprintf(GEN, 'OUTPUT:LOAD INF');
99  %
100 % Por defecto el Canal 1 aparece encendido, y el Canal 2 apagado
101 % Se enciende el canal 2 y se indica su impedancia de 50 Ohmios
```

```matlab
102  %
103  fprintf(OSC, ':CHANnel2:DISPlay 1');
104  %
105  fprintf(OSC, ':CHANnel2:IMPedance FIFty');
106  %
107  % Se autoescala la gr fica del osciloscopio
108  % y se ajusta el offset de los canales
109  %
110  fprintf(OSC, ':AUToscale');
111  fprintf(OSC, ':CHANnel1:OFFSet 0');
112  fprintf(OSC, ':CHANnel2:OFFSet 0');
113  %
114  %% ABRIMOS EL BUCLE
115  %
116  % Iniciamos el contador de iteraciones
117  %
118  i = 1;
119  %
120  % Usamos un 'while' porque MATLAB no deja reescribir el valor del
121  % indice 'i' de un bucle tipo 'for'
122  %
123  while i ≤ numpasos
124  %
125  % La frecuencia var a en cada paso
126  %
127      frequencies(i) = frequencyStart +(i * paso);
128  %
129      F = frequencies(i);
130  %
131  %Se le da al generador el nuevo valor de frecuencia
132  %
133      fprintf(GEN, 'FREQ %e',F);
134  %
135  %El osciloscopio mide para cada frecuencia
136  %
137      V1(i) = str2double(query(OSC, ':MEASure:VAMP? CHAN1'));
138      V2(i) = str2double(query(OSC, ':MEASure:VAMP? CHAN2'));
139      f(i) = str2double(query(OSC, ':MEASure:FREQ? CHAN1'));
140      arg(i) = str2double(query(OSC, ':MEASure:PHAS? CHAN2, CHAN1'));
141  %
142  % COMPROBACION: Si alguno de los valores esta fuera de escala y da
143  % error (9.9e+37), se autoescala y se repite la medida
144  %
145      if (V1(i) == 9.9e+37) || (V2(i) == 9.9e+37) || (f(i) == ...
              9.9e+37) || (arg(i) == 9.9e+37)
146  %
147      fprintf(OSC, ':AUToscale');
148      fprintf(OSC, ':CHANnel1:OFFSet 0');
149      fprintf(OSC, ':CHANnel2:OFFSet 0');
150  %
151  % Se reescribe el contador para sobreescribir la ultima medida,
152  % que ha sido erronea
153  %
154      i = i — 1;
155  %
156  % Se ignora el resto del bucle, volvemos al principio
157  %
```

```matlab
158        continue;
159    end
160    %
161    % CALCULO IMPEDANCIA AQU
162    %
163    % No se definen como arrays propiamente dichos
164    % porque sus componentes ya son arrays
165    %
166    X = (R.*(((V1./V2).*cosd(arg)) - 1));
167    Y = (R.*(V1./V2).*sind(arg));
168    Z = (sqrt((X.^2) + (Y.^2)));
169    %
170    % Se actualiza el contador
171    %
172    i = i + 1;
173    end
174    %
175    %% FICHERO DE DATOS
176    %
177    % Indicamos la direccion y etiqueta de guardado
178    %
179    fid1 = [directorio '\' etiqueta '.txt'];
180    %
181    % Abrimos el fichero
182    %
183    file1 = fopen(fid1,'wt');
184    %
185    fprintf(file1,'V1 V2 f arg X Y Z\n');
186    %
187    fprintf(file1,'%e %e %e %e %e %e %e \n', [V1; V2; f; arg; X; Y; Z]);
188    %
189    fclose(file1);
190    %
191    %% REPRESENTACI N GR FICA
192    %
193    % Ploteamos
194    plot (f,X,'g--',f,Y,'b--',f,Z,'r'); title ('Z-f Curve'); xlabel ...
            ('f (Hz)'); ylabel ('Z (Ohm)');
195    legend({'Parte Real','Parte Imaginaria','Impedancia Compleja'});
196    grid on; hold on;
197    % %
198    % % Guardamos la figura
199    % %
200    figura = [directorio '\' etiqueta '.png'];
201    saveas(gcf,figura)
202    %
203    %% FINALIZACI N DEL PROGRAMA
204    %
205    % Esperamos a que el script termine la medida
206    %
207    fprintf(GEN,'*WAI');
208    %
209    % Dejamos los aparatos con sus valores por defecto
210    %
211    fprintf(GEN,'*RST');
212    fprintf(OSC,'*RST');
213    %
```

```
214  % Cerramos Generador y Osciloscopio
215  %
216  fclose(GEN);
217  fclose(OSC);
218  %
```